Uncertainty Analysis of NASA Glenn's 8- by 6-foot Supersonic Wind Tunnel

Julia E. Stephens, Ph.D.*
HX5 Sierra, Cleveland, OH, 44070, USA

Erin P. Hubbard†
Jacobs, Cleveland, OH, 44070, USA

Joel A. Walter, Ph.D.‡
Jacobs, Bingham Farms, MI, 48025, USA

Tyler McElroy§
Jacobs, Tullahoma, TN, 37389, USA

An analysis was performed to determine the measurement uncertainty of the Mach Number of the 8- by 6-foot Supersonic Wind Tunnel at the NASA Glenn Research Center. This paper details the analysis process used, including methods for handling limited data and complicated data correlations. Due to the complexity of the equations used, a Monte Carlo Method was utilized for this uncertainty analysis. A summary of the findings are presented as pertains to understanding what the uncertainties are, how they impact various research tests in the facility, and methods of reducing the uncertainties in the future.

Nomenclature

Φ	Ratio between balance chamber static pressure and bellmouth total pressure
b_x	Systematic standard uncertainty of variable x
$d_2(n)$	Statistical weighting factor for small samples; value is based on sample size, n
M	Calculated test section Mach number
P_{bar}	Barometric pressure, psia
$P_{S,arr}$	Static pressure as measured by the transonic array, psia
$P_{S,bal}$	Static pressure in the balance chamber, psia
$P_{S,cyl}$	Static pressure as measured by the cone-cylinder for calibration, psia
$P_{S,ts}$	Calibrated static pressure in the test section, psia
$P_{T,2,arr}$	Total pressure downstream of a normal shock as measured by the transonic array for calibration (supersonic range), psia
$P_{T,2,ts}$	Calibrated total pressure downstream of a normal shock, psia
$P_{T,arr}$	Total pressure as measured by the transonic array for calibration (subsonic range), psia
$P_{T,bm}$	Total pressure in the bellmouth, psia
$P_{T,ts}$	Calibrated total pressure in the test section, psia
s_x	Random standard uncertainty of variable x
u	Standard uncertainty: an estimate of the standard deviation of the parent population from which a particular error originates
UPC	Uncertainty Percent Contribution

*Mechanical Engineer, AIAA Member.
†Mechanical Engineer, AIAA Member.
‡Mechanical Engineer, AIAA Member. Engineering Specialist
§Mechanical Engineer, AIAA Member.

I. Introduction

As advancements in science and engineering continue, the measurable desired improvements to technology become smaller. For example, aircraft engine companies hope to achieve 1% increases in efficiency with design changes. In order to measure these improvements, it is critical that the actual value of measurements are known to within these small boundaries.

Researchers continue to inquire about the uncertainties of the facilities in which tests are performed. Depending on the type of test, different aspects of uncertainty are of particular interest. For example, researchers wishing to compare test results with CFD results will care about facility offsets, while researchers looking for small measurement changes corresponding to design modifications are interested in facility repeatability. Due to this desire to understand the facility uncertainties, an effort is underway at the NASA Glenn Research Center to quantify and characterize the uncertainties of the facility set point parameters and other facility variables of interest.

Uncertainty analysis is a continually evolving field. As interest in the analysis process grows and computational processing improves, the process continues to be refined. The ASME Test Uncertainty Standard,[1] AIAA Standard for Wind Tunnel Test Uncertainty,[2] ISO Guide to the Expression of Uncertainty in Measurement,[3] and NASA Measurement Uncertainty Analysis Principles and Methods Handbook[4] are all useful resources when performing an analysis.

Data used for this analysis was obtained during a calibration in 1996-1997.[5] The uncertainty analysis was performed in 2014-2015. The objective was to determine the uncertainty in the free stream Mach number, as well as uncertainties in other free stream variables of interest (Reynolds number, air speed, dynamic pressure, static pressure, total pressure, static temperature, and total temperature). In addition to determining the overall uncertainties, the parameters that drive these uncertainties were also identified, as well as possible ways to improve the determined uncertainty. This paper discusses the process used to determine the uncertainty of the calculated Mach number, the primary drivers to this uncertainty, and methods to potentially lower this uncertainty. The actual values are not discussed, as they continue to change as improvements based on the analysis are implemented. More details on the analysis process, the findings for other calculated variables, and current uncertainty estimates are available in the NASA Contractor Report on the 8- by 6-foot SWT uncertainty analysis.[6]

II. Description of 8- by 6-foot Supersonic Wind Tunnel

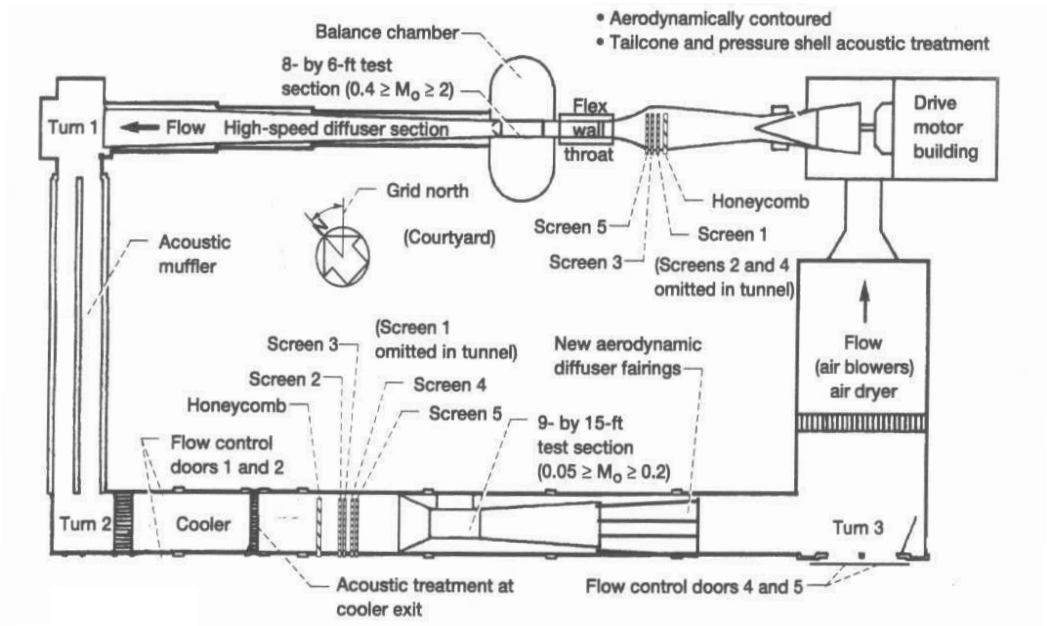

Figure 1: Overview of 8- by 6-foot Supersonic Wind Tunnel.

The 8- by 6-foot Supersonic Wind Tunnel (SWT) at the NASA Glenn Research center is an atmospheric, continuous flow wind tunnel. A schematic of the facility is shown in Figure 1. During standard operations, airflow is driven by a 7-stage compressor utilizing three 29,000-hp motors located in the drive motor building. The test section is 8 feet tall and 6 feet wide, with no divergence over the test section length. The test section is divided in to two testing sections: a solid wall supersonic flow region 9 feet 1 inch in length, and a porous wall transonic region 14 feet 5 inches in length. The Mach number range for the transonic test section is 0.25 to 2.0. Six configurations for the transonic test section are defined based on the length of the porous area used and porosity of the test section surfaces. This paper presents the results for the most commonly used configuration, which is the 14 foot long test section with 5.8-percent-porosity. For information on the other five configurations, see the NASA CR on the analysis.[6]

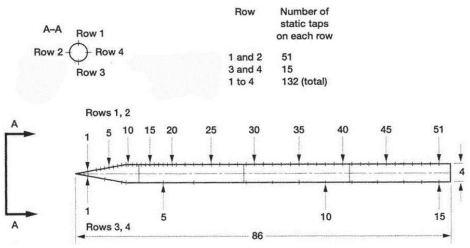

Figure 2: Instrumentation for the 4-inch cone-cylinder used during calibration.

The facility operating conditions are set by controlling compressor speed, flexible wall position, balance chamber pressure (test section bleed) and shock door position. The set point is determined predominantly by the ratio of the static pressure in the balance chamber to the total pressure in the bellmouth. To obtain these measurements, four static pressure measurements are taken at various locations in the balance chamber and are averaged to give $P_{S,bal}$. Two wall-mounted rakes near the exit of the bellmouth on the north and south tunnel walls acquire a total of eight total pressure measurements, which are averaged to give $P_{T,bm}$. More details on the facility operation can be found in the facility manual.[7]

The 8- by 6-foot SWT was calibrated in 1997[5] to provide facility-to-test-section relationships for the test section static pressure ($P_{S,ts}$), test section total pressure ($P_{T,ts}$), and test section total pressure downstream of a normal shock ($P_{T,2,ts}$). The calibration instrumentation used to collect test section data consisted of a cone-cylinder and a transonic array. The 4-inch diameter, 86-inch long cone-cylinder, shown in Figure 2, has four rows of static pressure taps. Rows 1 and 2 have 51 static taps each, while rows 3 and 4 have 15 static taps each.

The instrumentation on the transonic array includes 5 five-hole flow angularity probes, 6 Pitot-static probes and 11 thermocouples. A schematic of the instrumentation on the array is shown in Figure 3. The array is sting-mounted to a transonic strut in the facility and has wall plates at both ends for additional support. The vertical height of the array can be set to 5 different heights, from 24 to 72 inches in 12-inch increments, with 48 inches being the tunnel center-line. The axial position of the array is also variable. For configuration 1, the 138.4-inch station is used, placing the center-line of the flow angularity probes approximately at the center-line of the Schlieren window blanks.

When operating the 8- by 6-foot SWT, nominal conditions for compressor speed, flexible wall position, and shock door positions are set. The ratio of the balance chamber to bellmouth pressures is also set to a nominal value based on the tables in the facility operations manual.[7] This ratio is defined as

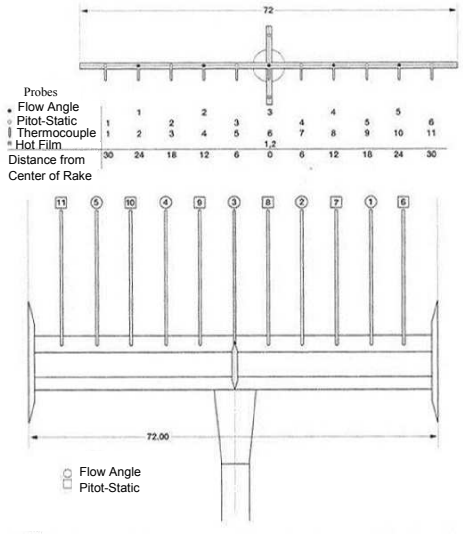

Figure 3: Instrumentation on the transonic array used during calibration. All dimensions are in inches.

$$\Phi = \frac{P_{S,bal}}{P_{T,bm}}. \tag{1}$$

The average of all static pressure measurements over the aft half of the cylinder, defined as $P_{S,cyl}$, is used

to represent test section static pressure ($P_{S,ts}$) to determine calibration curve coefficients using

$$P_{S,ts} = P_{T,bm} \cdot (B_0 + B_1 \cdot \Phi + B_2 \cdot \Phi^2 + B_3 \cdot \Phi^3 + B_4 \cdot \Phi^4 + B_5 \cdot \Phi^5 + B_6 \cdot \Phi^6). \tag{2}$$

Readings from the outer two pressure probes on each end of the array were not used in the calibration to assure boundary layer effects were not present in the data. The innermost 4 Pitot-static and 3 flow angularity probe readings taken at the center-line vertical array height were averaged to produce $P_{T,arr}$ and $P_{S,arr}$. Note that in supersonic flow, the pressure measured by the array probes is the total pressure downstream of a normal shock, and is denoted by $P_{T,2,arr}$. Calibration curve-fit coefficients are determined using these average array measurements, which represent test section total pressure ($P_{T,ts}, P_{T,2,ts}$). Subsonically, the curve is defined as

$$P_{T,ts} = A_0 + A_1 \cdot P_{T,bm} + A_2 \cdot P_{T,bm}^2, \tag{3}$$

and supersonically total pressure coefficients are given by

$$P_{T,2,ts} = P_{T,bm} \cdot (AS_0 + AS_1 \cdot \Phi + AS_2 \cdot \Phi^2 + AS_3 \cdot \Phi^3 + AS_4 \cdot \Phi^4 + AS_5 \cdot \Phi^5 + AS_6 \cdot \Phi^6). \tag{4}$$

Using test-time facility measurements and the calibrated values for $P_{S,ts}$, $P_{T,ts}$, and $P_{T,2,ts}$, the test section Mach number is calculated in the subsonic range by

$$M_{ts} = \sqrt{\frac{2}{\gamma - 1}\left[\left(\frac{P_{S,ts}}{P_{T,ts}}\right)^{-\frac{\gamma-1}{\gamma}} - 1\right]}, \tag{5}$$

where γ is the ratio of specific heats, 1.4 for air. In the supersonic range, M_{ts} is solved for iteratively using the Rayleigh Pitot formula:[8]

$$\frac{P_{T,2,ts}}{P_{S,ts}} = \left[\frac{(\gamma+1)M_{ts}^2}{2}\right]^{\frac{\gamma}{\gamma-1}} \left[\frac{\gamma+1}{2\gamma M_{ts}^2 - (\gamma-1)}\right]^{\frac{1}{\gamma-1}}. \tag{6}$$

The following section outlines the steps used to determine the uncertainty of the Mach number calculated using the above described data and equations.

III. Measurement Uncertainty Analysis

The general process of the analysis used is described in this section. The methods of dealing with non-ideal data conditions are also discussed. The final values of the various uncertainty sources are not included. More details on the analysis process and final values used are contained in the NASA CR.[6]

A. Identify Error Sources

The uncertainty of a value is an estimate of the range within which the actual value of an (unknown) error is believed to fall.[9] An elemental error is the most basic error in a measurement. A standard uncertainty, u is an estimate of the standard deviation of the population which results in this error, or the uncertainty of this measurement. Standard uncertainties for each error in a calculation propagate through the calculation and result in the uncertainty, U, of the result.

Uncertainty texts group the elemental uncertainties for ease of investigation. The ISO Guide to the Expression of Uncertainty in Measurement[3] classifies uncertainties as Type A and Type B. Type A is based on direct observation and statistical analysis, while Type B is based on operator experience, manufacturer documentation, or another means. Other texts[1,2,4,9] classify uncertainties as "random" and "systematic." Systematic errors create an offset from the actual value (X_{true}) to the "nominal" value (X_{nom}), while random errors cause a random variation typically following a Gaussian distribution about the nominal value. Figure 4 shows the effect each of these error types has on a measured value.

Random standard uncertainty, s_x, characterizes the repeatability of a measurement of variable x. In other words, a population of random errors of measurement x has a standard deviation of s_x. Due to the nature of random errors, increasing sampling time and/or number of discrete repeats in the data set reduces the effect of random uncertainty on test data.

Systematic standard uncertainty, b_x, characterizes a bias in the measurement of variable x. Examples of systematic error sources can include instrumentation and facility calibration, operator interaction, facility behavior such as spatial non-uniformity, and math models such as curve-fits. Tunnel calibrations, comprised of both random and systematic uncertainties when calibration tests are performed, become fossilized[10] as a systematic uncertainty when a customer uses the resultant calibration curves for test-time analysis.

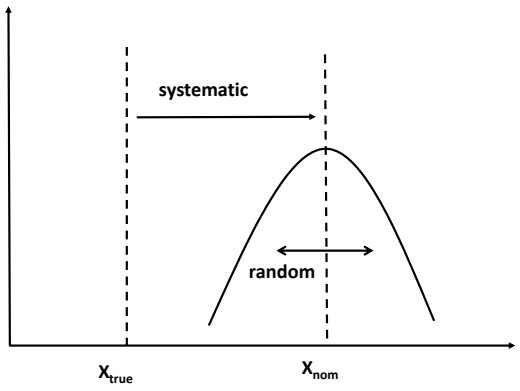

Figure 4: Effects of systematic and random errors on a measurement.

Correlated errors occur when there is some type of link between two or more measurements. One example of a random correlation error is two total pressure probes taking measurements in a slightly unsteady flow, where test section conditions may change on a time basis; that variability appears as random correlated errors, present in any simultaneous measurements of the probes. On the other hand, measurements from multiple instruments that are calibrated by the same process and instrumentation share systematic correlated errors; any offset due to calibration appears in all measurements from these instruments.

Distinguishing between uncertainty sources as random and systematic can be useful in determining which changes could reduce a facility's uncertainty. Additionally, categorizing the uncertainties in this manner may help researchers understand if the uncertainties will affect their data. For example, a test in which a researcher hopes to compare the results with CFD models requires low systematic uncertainty but may not be bothered by high random uncertainty, while a researcher looking for small changes in results due to model modification requires low random uncertainty but may not be bothered by an offset in their data.

B. Uncertainty Propagation

This uncertainty analysis uses a "bottom-up" approach, following the uncertainty flow from the point of measurement to calculated variables of interest. The analysis begins by determining elemental uncertainty estimates of the instrumentation used for measurements, then determines the random and other systematic uncertainties associated with measurements and the facility. As calibrations and calculations (or assumptions) are made, associated uncertainties are also determined, and all uncertainties are propagated to obtain the resulting uncertainty in the value of interest.

Variables from the data reduction that determine the free stream Mach number in the 8- by 6-foot SWT are the calibrated test section static pressure, $P_{S,ts}$, total pressure in the subsonic range, $P_{T,ts}$, and total pressure downstream of a normal shock in the supersonic range, $P_{T,2,ts}$. These calibrated values are calculated during a customer test using facility measurements of average total pressure in the bellmouth, $P_{T,bm}$, average static pressure in the balance chamber, $P_{S,bal}$, and total and static pressure calibration regression coefficients. An example of this data flow for supersonic Mach numbers is shown in Figure 5. All measured pressures are differential and referenced to barometric pressure, P_{bar}, to produce absolute pressures.

Contributors to uncertainty in the test section Mach number are, therefore, random and systematic uncertainties in the measured values of $P_{T,bm}$ and $P_{S,bal}$, systematic uncertainty in the reference pressure P_{bar} (random uncertainty is assumed to be negligible), and fossilized systematic uncertainty from the calibration curves used to determine values of $P_{S,ts}$, $P_{T,ts}$, and $P_{T,2,ts}$. Each of these calibrations contributes a single systematic uncertainty to calculated test section Mach number. This systematic uncertainty contains all of the uncertainties of the calibration (random and systematic) combined and fossilized. As an example, Figure 6 shows static pressure calibration uncertainties that combine to become the single uncertainty contribution to $P_{S,ts}$ due to calibration, which propagates to the uncertainty of M_{ts}. An example of uncertainty flow for M_{ts} is shown for the supersonic range in Figure 7.

It should be noted that because the analysis is based on the data obtained during a calibration, all of the quoted uncertainties for all variables of interest are considered calibration point uncertainties, centered on the tunnel's x and y axes and axially defined by the configuration. Results do not include uncertainties due to test time uncertainty considerations such as test section effects or spatial uniformity.

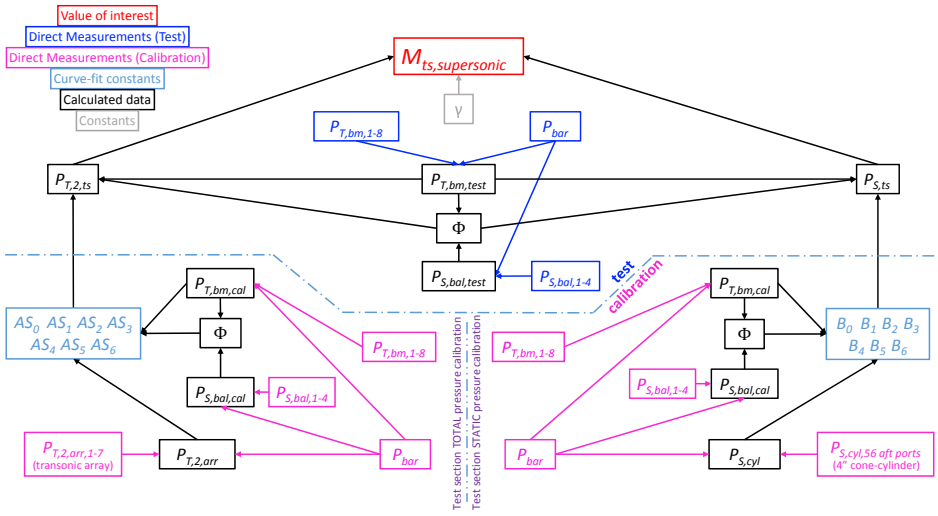

Figure 5: Data flow from measured value to calculated Mach number for supersonic flow.

C. Instrumentation Level Uncertainties

The uncertainty of a system begins with the instrumentation used to obtain the measured values. This analysis uses the Measurement ANalysis Tool for Uncertainty in Systems (MANTUS), an Excel® based tool which allows the user to break down the overall measurement into component parts, or "modules", to easily handle the analysis of multi-level instrumentation systems. A module can be configured to represent a specific function of a single component, or multiple components can be summarized into one module. The overall system is then assembled from multiple modules within MANTUS, allowing for propagation of uncertainties using the Taylor Series Method[1–4,9] to ultimately produce the final uncertainty of the measurement. This process is depicted in Figure 8. More details on the MANTUS tool can be found in the MANTUS CR.[11]

For this analysis, MANTUS is used to quantify the systematic uncertainties of pressure measurement instrumentation. Pressure measurements in the 8- by 6-foot SWT are obtained using ±15-psid pressure units within the S3200 Electronic Scanning Pressure (ESP) system. Using the methodology outlined in the NASA MUA Handbook,[4] MANTUS breaks down the pressure system into modules such as the sensor, signal conditioner, analog to digital convertor, and data processor. The cumulative uncertainty effects of the different modules on the measurements being taken were determined. This output accounts for multiple variables present in each measurement subsystem, producing a mathematically verifiable instrumentation model.

All pressures considered in this analysis share a common ±15-psid pressure calibration unit and were calibrated to the same reference pressure. As a result, the instrumentation calibration errors are considered fully correlated between all pressure measurements within a calibration cycle. Throughout this analysis, correlated uncertainties from pressure instrumentation are considered as a unit rather than separated into each specific variable's contribution.

Although the barometric pressure is not directly shown in any of the calculations for the variables of interest, it is present in the data reduction and chain of uncertainty propagation since it is added to the measured differential pressures to produce absolute pressures. The barometric pressure is measured by a high accuracy transducer that is part of the pressure calibration unit for the ESP system.

All of the instrumentation uncertainties determined by MANTUS can be found in the NASA CR.[6]

D. Uncertainty due to Calibrations of Free Stream Quantities

Any time a calibration is performed, the errors that were present at the time of the calibration test are "fossilized" into the calibration curve. All uncertainties contributing to the calibration form a combined systematic uncertainty and apply to any value calculated by the calibration curve, as shown in Figure 7. Therefore, the calibrations for this facility each require an uncertainty analysis evaluating systematic uncertainties in all instrumentation (facility and calibration hardware), random uncertainties in all measured

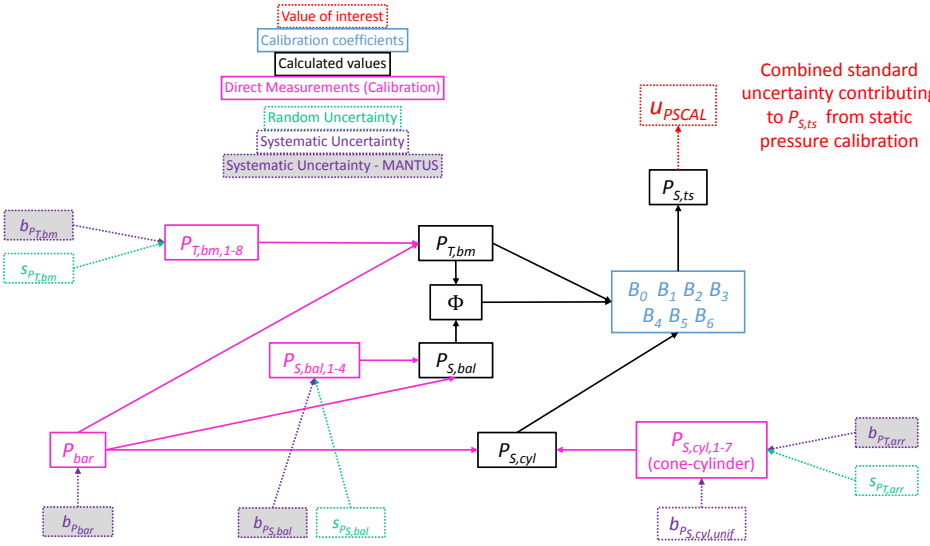

Figure 6: Flow chart depicting the flow of uncertainty for static pressure calibration.

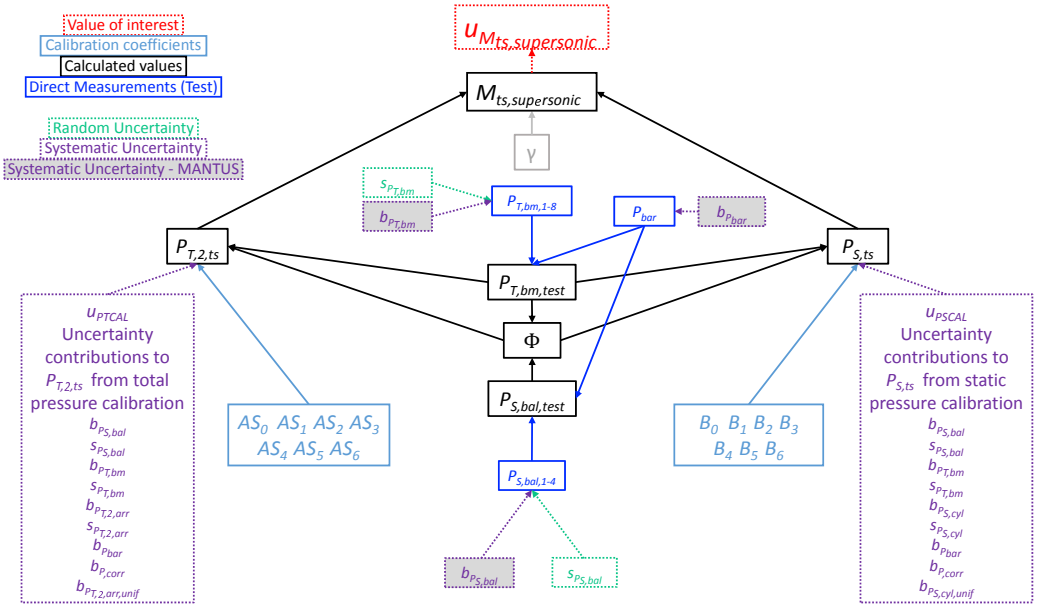

Figure 7: Flow chart depicting the propagation of uncertainties in Mach number calculation for supersonic flow.

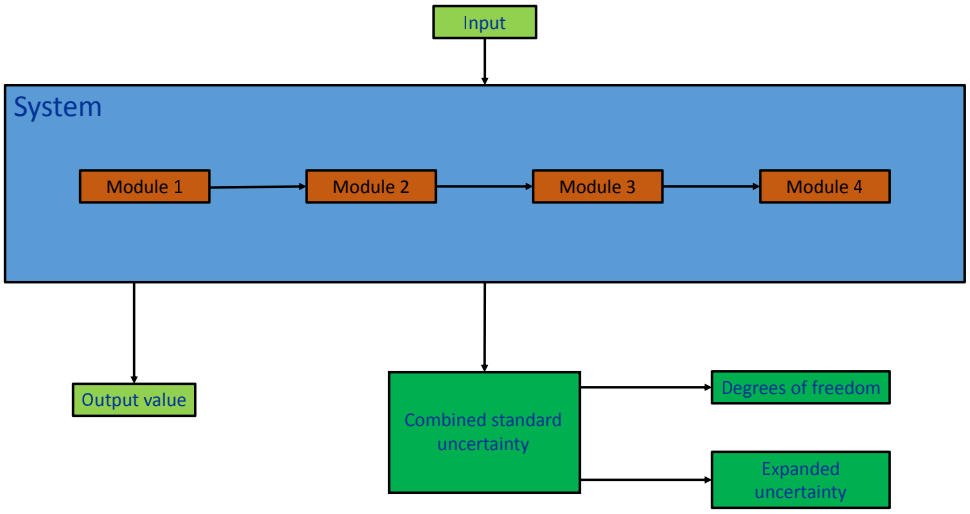

Figure 8: Instrumentation level uncertainty analysis information flow.

variables (facility and calibration measurements), and systematic uncertainty due to spatial non-uniformity. A visual example of how these uncertainties apply to calibration measurements is shown for the static pressure calibration in Figure 6.

Measurements used in the calibrations include facility measurements ($P_{T,bm}$, $P_{S,bal}$, and P_{bar}) and test section measurements (cone-cylinder: $P_{S,cyl}$ and transonic array: $P_{T,arr}$, $P_{T,2,arr}$). The instrumentation level uncertainties for all measurements are estimated using MANTUS.

The random uncertainty of each measurement is due to the inability to obtain the exact same measurement twice. This can be a result of effects such as noise, dynamic behavior, or unidentified systematic uncertainties that present as random uncertainties. Generally, this uncertainty can be estimated using the mean

$$\bar{X} = \frac{1}{N}\sum_{i=1}^{N} X_i, \tag{7}$$

and standard deviation

$$s_X = \sigma_X = \sqrt{\frac{1}{N-1}\sum_{i=1}^{N}(X_i - \bar{X})^2} \tag{8}$$

of a sample population of measurements at a given tunnel condition. N is the number of individual measurements of variable X.

Ideally enough data is available to use Equation 8 to obtain a valid random uncertainty estimate for a given variable for each nominal tunnel set point (about ten data points[9]). In some tunnels, where statistical process control is implemented or where calibrations are regularly performed, this may be a good option. Unfortunately, a plethora of repeat data is not a luxury many wind tunnel data analysts enjoy. Understandably, data sets are often small due to high costs of running facilities, and few repeat readings are available for analysis. The data set for this analysis is limited to data collected during the calibration in 1997.[5] The calibration test matrix consisted of only one or occasionally two Mach range sweeps for any given hardware setup. While two to three back-to-back, time-averaged data points are available for each reading in a Mach range sweep, these are averaged and considered a single reading to assure the time scale is representative of factors that have significant influence on random uncertainty in the data.[9]

When an insufficient number of distinct repeat data points are available to use Equation 8, s_x can be estimated by converting the range of the available data from a biased to an unbiased estimator of the standard deviation:[12]

$$s_X = \sigma_X \approx= \frac{X_{max} - X_{min}}{d_2(n)}, \tag{9}$$

where X_{max} is the maximum value in the sample, X_{min} is the minimum value, and d_2 can be derived as a function of n, the number of readings in the sample, assuming a normal probability distribution. Values of d_2 for small sample sizes are provided in Table 1.

n	2	3	4	5	6	7	8	9
$d_2(n)$	1.128	1.639	2.059	2.326	2.534	2.704	2.847	2.970

Table 1: Values for statistical estimation factor $d_2(n)$ for n samples

During calibration, the transonic array obtained two distinct repeated data samples for approximately half of the tunnel's set points distributed across the Mach range at different times during the test. When Equation 9 is applied to $P_{T,arr}$, $P_{T,2,arr}$, and $P_{S,arr}$, results shown in Figure 9 are obtained. The similar behavior indicates a random correlation between these variables. The correlation is believed to be present due the process of setting the tunnel condition based on Φ and its effect on the relationship between static and total pressure within the test section. For example, total and static pressure may vary upward and downward together, perhaps following changes in barometric pressure, even as Φ remains constant. Not accounting for this correlation results in artificially inflated uncertainty estimates.

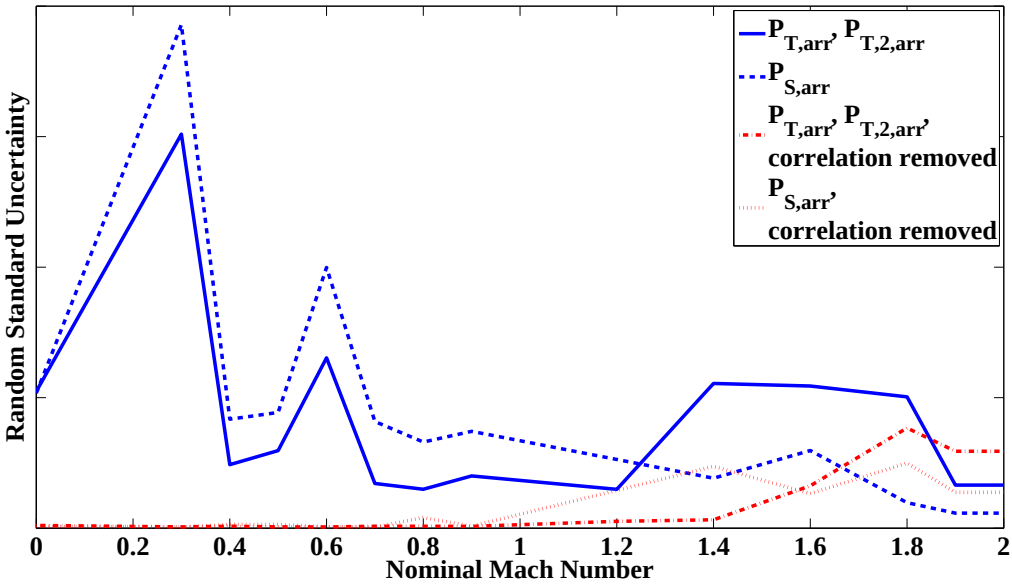

Figure 9: Standard deviations in $P_{T,arr}$, $P_{T,2,arr}$ and $P_{S,arr}$ for test section configuration 1, with and without correlations removed

To remove the effects of this correlation, an "expected" test section pressure based on facility measurements and calibration curves for $P_{S,ts}$, $P_{T,ts}$, and $P_{T,2,ts}$ is determined. The difference between the measured and expected value for each of the two available data points (the residuals) are evaluated at each tunnel set point. The d_2 factor is applied to those results, providing modified estimates of random standard uncertainty for $P_{T,arr}$, $P_{T,2,arr}$, and $P_{S,arr}$ are obtained. The result is shown in Figure 9. The reduction in the subsonic region is about a factor of 100.

Only one sweep through the Mach range was performed during the static pressure calibration. Therefore, no repeat data points were acquired for cylinder static pressure $P_{S,cyl}$. Since static pressure data was acquired by the transonic array with similar pressure probes in similar locations and tunnel conditions, the random uncertainty in static pressure measured by the cylinder is estimated using the available array data, $P_{S,arr}$.

If, in the future, more data is obtained with the cylinder, the random uncertainty should be estimated using cylinder data.

E. Random Uncertainty in Facility Measured Values

Facility measurements in the data reduction chain for variables of interest in the 8- by 6-foot SWT consist of $P_{T,bm}$, $P_{S,bal}$, and P_{bar}. Random uncertainty in P_{bar} is assumed to be negligible for this analysis.

As described above, the operating condition of the facility is determined in part by setting Φ, the ratio of $P_{S,bal}$ to $P_{T,bm}$. As a result, for a given nominal Mach number setting, the two measurements can vary widely even when the same ratio is obtained. This allows values of $P_{T,bm}$ and $P_{S,bal}$ to vary significantly, creating a random correlation effect between the variables. This presents in the analysis as seemingly high uncertainty estimates when straight standard deviations are taken using Equation 9.

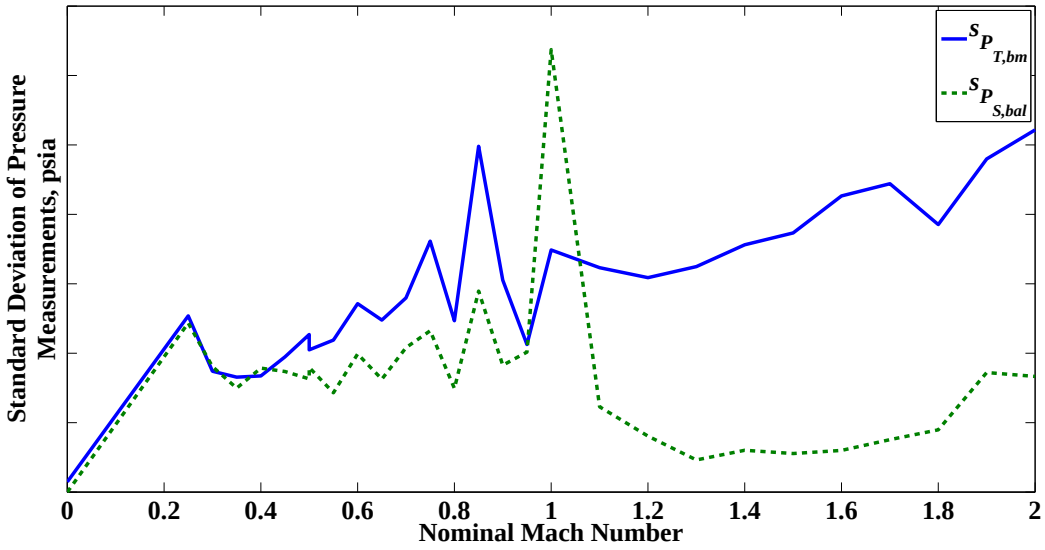

Figure 10: Standard deviations of $P_{T,bm}$ and $P_{S,bal}$ for test section configuration 1.

Along with being unrealistically high, these uncertainties appear to trend together, as shown in Figure 10, verifying the suspected presence of a random correlation between the parameters. As with the correlation between $P_{S,ts}$ and $P_{T,ts}$, random correlation between $P_{S,bal}$ and $P_{T,bm}$ is accounted for by finding the difference between an "expected" or "nominal" value and the measured value. To determine the expected value, a linear curve-fit is created of the two variables using all available data at a certain tunnel set point and test section configuration. The standard deviation is estimated from those residuals of the difference between this expected value and the value measured for each variable. An example result using this technique to determine the standard deviation of $P_{S,bal}$ at Mach 0.8 and test section configuration 1 is shown in Figure 11. It is notable that since facility parameters are not dependent on test section hardware setup, there is more data available for facility measurements than for test section measurements.

The resulting random standard uncertainty estimates of $P_{S,bal}$ and $P_{T,bm}$ as a function of nominal Mach number are shown in Figure 12. Despite attempts to account for the correlation due to the ratio Φ described above, there still appears to be a random correlation present in these estimates. Preliminary analysis showed these parameters as driving the overall uncertainty in values of interest, so the correlations need to be addressed for an accurate understanding of the facility uncertainties.

The remaining random correlation effects between $P_{T,bm}$ and $P_{S,bal}$ are likely a result of tunnel operation. Small variations in the primary tunnel set point parameter, Φ, occur when operators attempt to achieve the same tunnel set points repeatedly. While this means that tunnel conditions may not be identical for repeat points, this does not mean conditions are assumed by facility personnel or customers to be the same; Φ is present in data reduction chains leading to $P_{T,ts}$, $P_{S,ts}$ and ultimately Mach number and other free stream quantities. Therefore, while the same precise tunnel condition may not be achieved for repeat measurements, the precise conditions are still known to within measurement uncertainty bounds for each point.

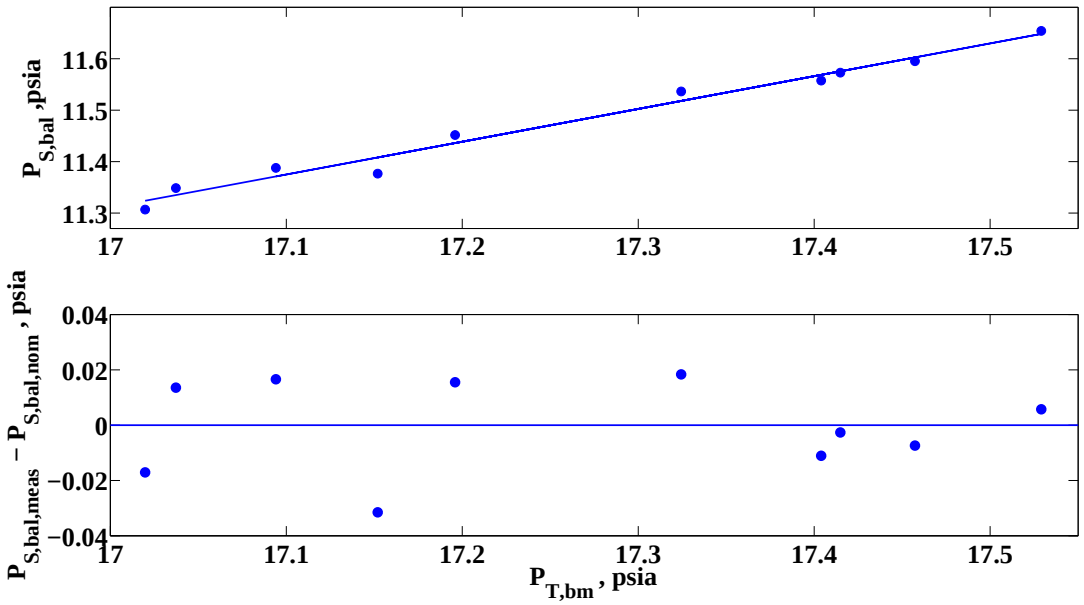

Figure 11: The relationship between $P_{S,bal}$ and $P_{T,bm}$ for test section configuration 1 at nominal Mach 0.8 tunnel setting. (top) Scatter represents $P_{S,bal}$ vs. $P_{T,bm}$, line represents linear curve-fit and a determined $P_{S,bal,nom}$; (bottom) $P_{S,bal}$ residuals

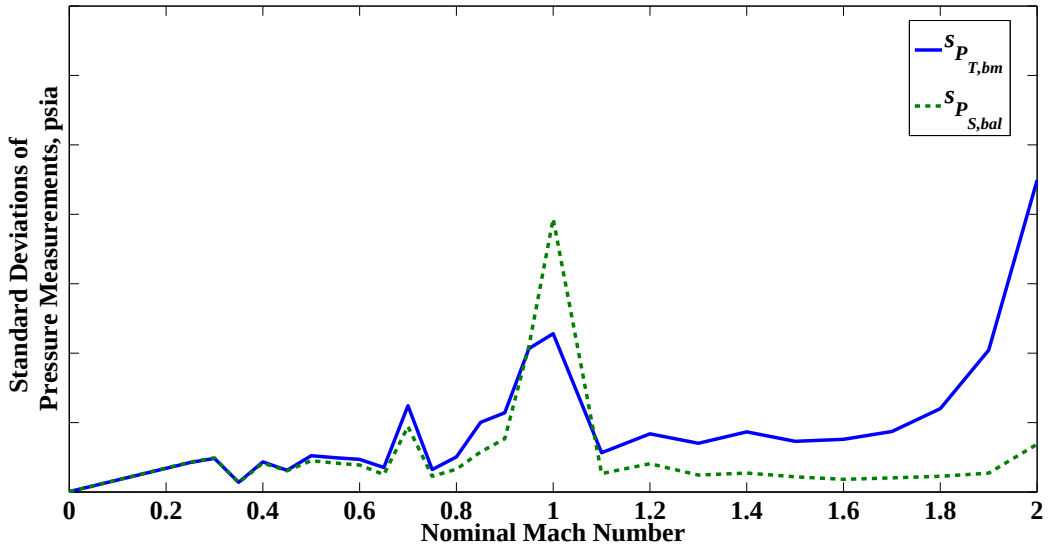

Figure 12: Standard deviations of $P_{T,bm}$ and $P_{S,bal}$, using residuals technique to remove random correlation effect

Without a way to further refine random uncertainty estimates for $P_{T,bm}$ and $P_{S,bal}$, an engineering judgment was made to use static pressure random standard uncertainty estimates from the array ($s_{P_{S,arr}}$) to estimate random uncertainty of static pressure in the balance chamber ($s_{P_{S,bal}}$). Likewise, total pressure estimates from the array ($s_{P_{T,arr}}$ and $s_{P_{T,2,arr}}$) are used to estimate random uncertainty of total pressure in the bellmouth ($s_{P_{T,bm}}$). These estimates are considered conservative since the test section environment where array pressures were measured are presumably more dynamic than the bellmouth and balance chamber probe locations. These results are used for all calibration simulations, as well as the test-time simulation.

F. Spatial Uniformity Uncertainty

Uncertainty due to spatial uniformity is determined by taking the standard deviation of the measurements across all ports used for the representative average test section measurement during calibration. For the static pressure calibration, this consists of 56 measurements along the aft portion of the cone-cylinder, the variation of which is assumed to be due to spatial non-uniformity. For total pressure, Equation 9 is applied to the seven center pressure measurements across the transonic array at the 48-inch rake height. These results are temporarily defined as "observed" spatial uniformity uncertainties.

When considering uncertainty due to spatial uniformity, it is important to verify that other error sources (instrumentation, random) are not also contributing to the observed results, and that the spatial uniformity uncertainty effects are isolated. Systematic uncertainty in instrumentation is cause for concern, as it can create an offset in the observed spatial uniformity uncertainty. However, because of the way pressure measurements were obtained through ESP for this data set, all of the instrumentation errors are correlated for $P_{S,cyl}$ and $P_{T,arr}$; therefore, instrumentation errors affect all simultaneous measurements equally and are not a factor when taking a standard deviation across the measurements at a given time and observed results are good estimates. For these parameters, random uncertainties are significantly smaller than the observed spatial uniformity and were deemed negligible contributors to the observed uniformity uncertainties.

G. Monte Carlo Simulation

To properly propagate the elemental uncertainties to the uncertainty of the calculated value of interest, an error model is necessary. The traditional model for propagating uncertainty is the Taylor Series Method (TSM), which is derived as a linearized Taylor series expansion about the true result from the data reduction equation. The true (but unknowable) result is then replaced by its estimate, i.e. the sum of the measured result and the error estimates (uncertainties). The complete derivation of the model is provided by Coleman and Steele.[9]

Due to the nature of complex or highly non-linear equations, the Taylor Series Method can become cumbersome to implement or may require assumptions to simplify equations, ultimately increasing the uncertainty in the final result. In such instances, the Monte Carlo Method (MCM) is useful as an uncertainty propagation technique. Approaches for using the MCM are detailed by Coleman and Steele,[9] and the method is standardized in the ISO Guide's supplement.[13] Details on both methods as used for this analysis are outlined in the NASA CR.[6]

Given the iterative calculations required to obtain the free stream Mach number in this facility, the MCM of uncertainty propagation was selected for this analysis. In summary, a Monte Carlo simulation begins with a data set representative of a typical test. A population of i synthetic data sets are produced by perturbing the data set by errors determined by elemental uncertainty estimates for each uncertainty contributor considered, and for each measured parameter.[14] Each of the i perturbed data sets are sent through the data reduction sequence, producing i calculations of any values of interest. Finally, the standard uncertainty of the calculated values are determined by taking the standard deviation of the perturbed results.

For this uncertainty analysis, an offline data reduction program replicates the actual data reduction script run within the Escort data acquisition system. MATLAB® is used because of its specialty in performing array calculations, which works well for a Monte Carlo simulation where thousands of iterations are often desired.

The simulation begins by randomly generating numbers along an appropriate probability distribution and scaling them by the random and systematic uncertainties of each variable. These populations of errors are applied to the appropriate measurements in an appropriate manner across all readings, ports, and i synthetic iterations of the test. This analysis uses $i = 10,000$ for the calibrations and $i = 100,000$ for simulations calculating uncertainties in variables of interest.

Once errors are applied to all measured values for each iteration of the test, the variables of interest are calculated using the synthetic data. This results in i calculations of any variable of interest. The standard deviation provides the desired overall uncertainty of the variable of interest. This process is depicted in Figure 13 as it applies to the subsonic total pressure calibration.

When possible, it is preferable to construct a Monte Carlo simulation program that follows an actual test as closely as possible. This approach usually makes it easier to follow the flow of data and introduce elemental errors in the appropriate places. To that end, Monte Carlo simulations are run for each of the calibration tests (static and total pressure). The results of each of these simulations provide the fossilized systematic uncertainties to be applied in the subsequent simulation of a customer test, where all variables of interest and their uncertainties are calculated. Finally, a coverage factor is applied to calculate the expanded uncertainties.

The code is written in such a way that elemental uncertainties can be flagged on or off. The flags allow one elemental uncertainty to be propagated at a time so that the effect of that uncertainty on the total uncertainty of a variable can be calculated. These sum as root sum squares to the total uncertainty of a variable (which is confirmed by performing the analysis with all uncertainties flagged on and obtaining the same result). Using these results, the percent contribution of each elemental uncertainty (or group of uncertainties, such as all instrumentation) to the overall uncertainty of the value of interest is observed (see Equation 10). More details on this process, including proper error propagation, are included in the NASA CR.[6]

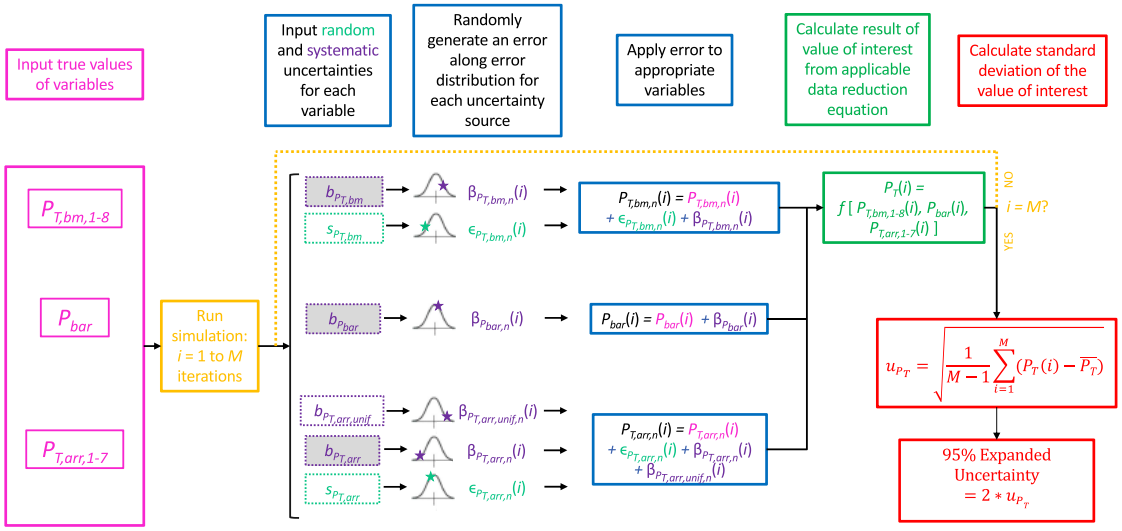

Figure 13: Overview of Monte Carlo Simulation for Uncertainty Analysis: Depicts analysis of total pressure calibration in subsonic range. Based on the method described by Coleman and Steel[9] page 72, Figure 3.4.

H. Analysis Limitations

Uncertainty results are only as good as the elemental uncertainty estimates that are propagated. The more pertinent data that is available for random, systematic, and spatial uniformity uncertainty estimates, the better the results of the analysis. This particular analysis is somewhat limited by its data set, which was designed to assess the mean behavior of the 8- by 6-foot SWT, rather than its dispersive behavior. Random uncertainty estimates are difficult to make due to a lack of repeat data over the appropriate time scales, and correlations between variables during normal operation have been observed but are difficult to account for with the existing data set. Additional runs during a calibration entry or perhaps a specially designed test would be required to refine the random uncertainty estimates.

IV. Results

To aid in communicating the impact of different uncertainty sources, the uncertainties are presented as uncertainty percent contributions (UPC), determined by:

$$\mathrm{UPC}_i = \frac{u_i^2}{u_{total}^2} \times 100, \tag{10}$$

where u_i is the uncertainty contribution to the variable of interest due to elemental uncertainty i, and u_{total} is the total uncertainty of the variable of interest, calculated by root-sum squaring the elemental uncertainty sources and confrimed by running the MCM simulation with all error sources flagged "on."

The percent contributions of random and systematic uncertainty to total uncertainty in M_{ts} are shown in Figure 14. With the current calibration data and analysis, the uncertainty is overwhelmingly driven by systematic uncertainty.

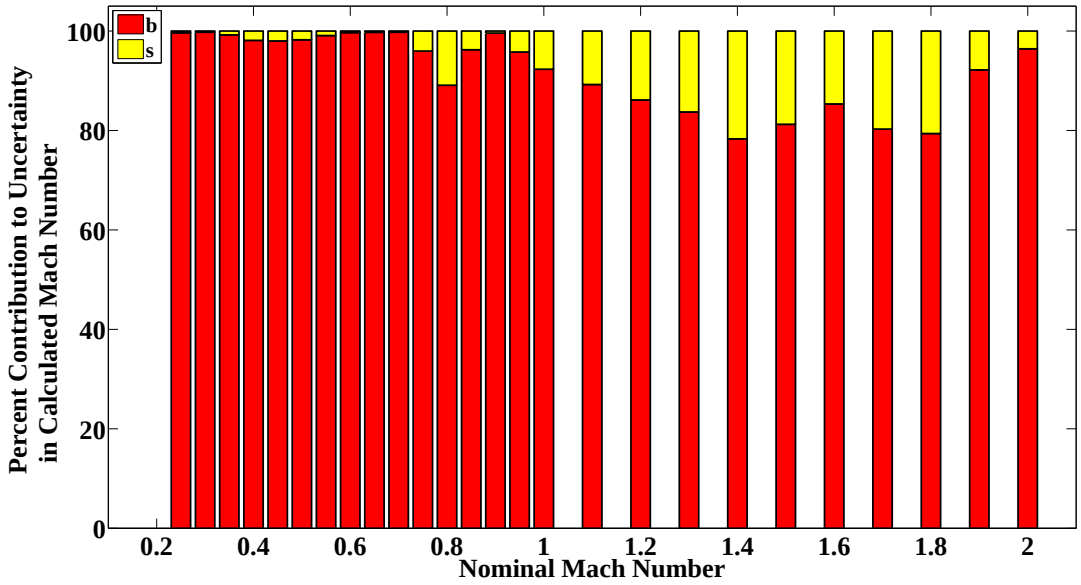

Figure 14: UPC random (s) and systematic (b) contributions to M_{ts} as a function of nominal Mach number for test section configuration 1. Red is the systematic uncertainty and yellow is the random uncertainty.

Looking at Equations 5 and 6, the elemental random uncertainties in $P_{T,bm}$ and $P_{S,bal}$ contribute to random uncertainty in Mach number. The UPC of these elemental uncertainties to the total random uncertainty in M_{ts} is shown in Figure 15. Random variation of the static pressure in the balance chamber overwhelmingly drives the random uncertainty in M_{ts} across most of the range. Similar results were observed in the National Transonic Facility.[14]

The combined systematic uncertainty in M_{ts} is due to the uncertainty in total and static pressure calibrations (b_{PTCAL} and b_{PSCAL}), and instrumentation uncertainties in test-time total pressure in the bellmouth and static pressure in the balance chamber measurements (combined as $b_{P,Inst}$). A bar plot of the UPCs of the elemental systematic uncertainties contributing to M_{ts} are shown in Figure 16. Uncertainty due to instrumentation contributes very little, while the primary contributor to systematic uncertainty in Mach number is the static pressure calibration.

Each calibration uncertainty contribution from Figure 16 can be further broken down, as shown in Figures 17-18. Note that in the supersonic range, the total pressure downstream of a normal shock is measured by the array ($P_{T,2,arr}$). For simplicity, $P_{T,2,arr}$ and $P_{T,2,ts}$ are shown on the same charts as $P_{T,arr}$ and $P_{T,ts}$. Subsonically the primary driver to both static and total pressure calibrations is instrumentation. Supersonically, the calibration uncertainties are driven by pressure uniformity. So, even though instrumentation is not a driver during test time, upgrades to instrumentation must still be considered. Instrumentation uncertainty

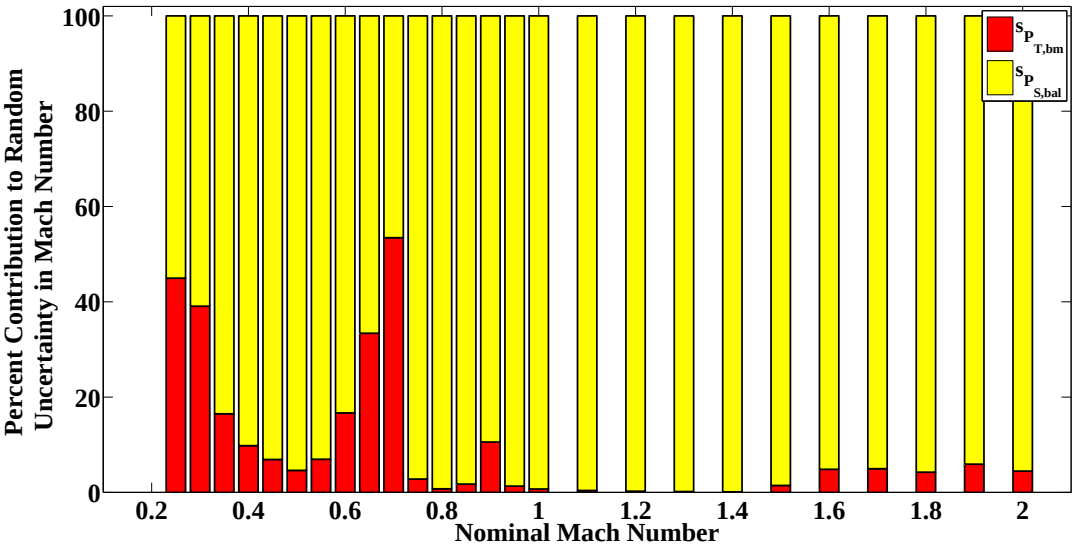

Figure 15: Random UPC of M_{ts} as a function of nominal Mach number for test section configuration 1. Red is the random uncertainty of the total pressure in the bellmouth ($s_{P_{S,bal}}$), yellow is the random uncertainty of the static pressure in the balance chamber ($s_{P_{T,bm}}$).

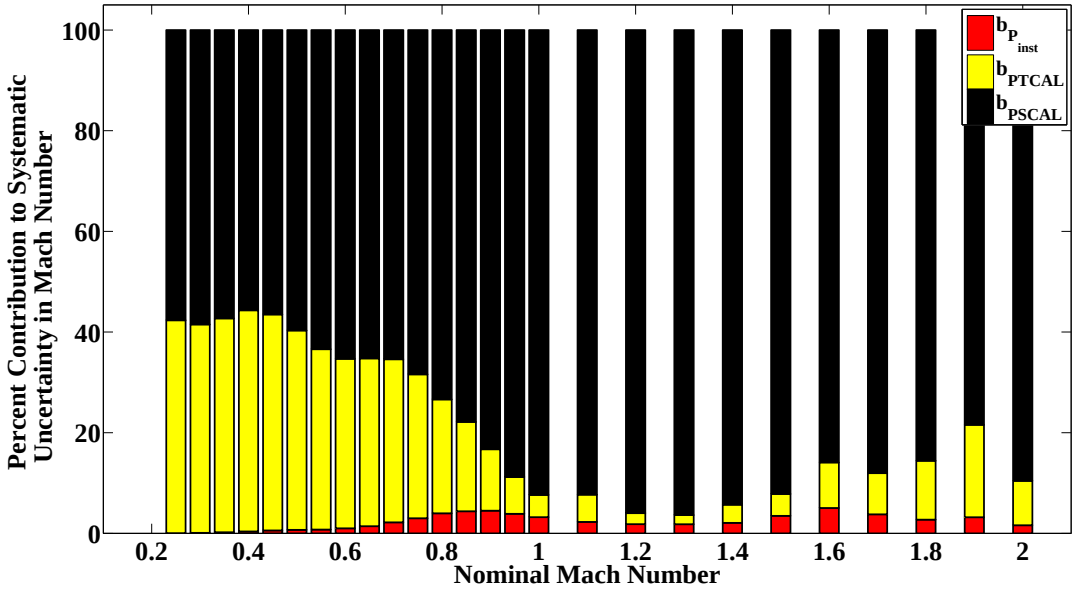

Figure 16: Systematic UPC for M_{ts} as a function of nominal Mach number for test section configuration 1. Red is the systematic uncertainty due to pressure instrumentation ($b_{P_{inst}}$), yellow is the systematic uncertainty due to total pressure calibration (b_{PTCAL}), and black is the systematic uncertainty due to static pressure calibration (b_{PSCAL}).

can also be broken down to the individual modules, as shown in Figure 19. The instrumentation uncertainty is overwhelmingly driven by the pressure scanner uncertainty.

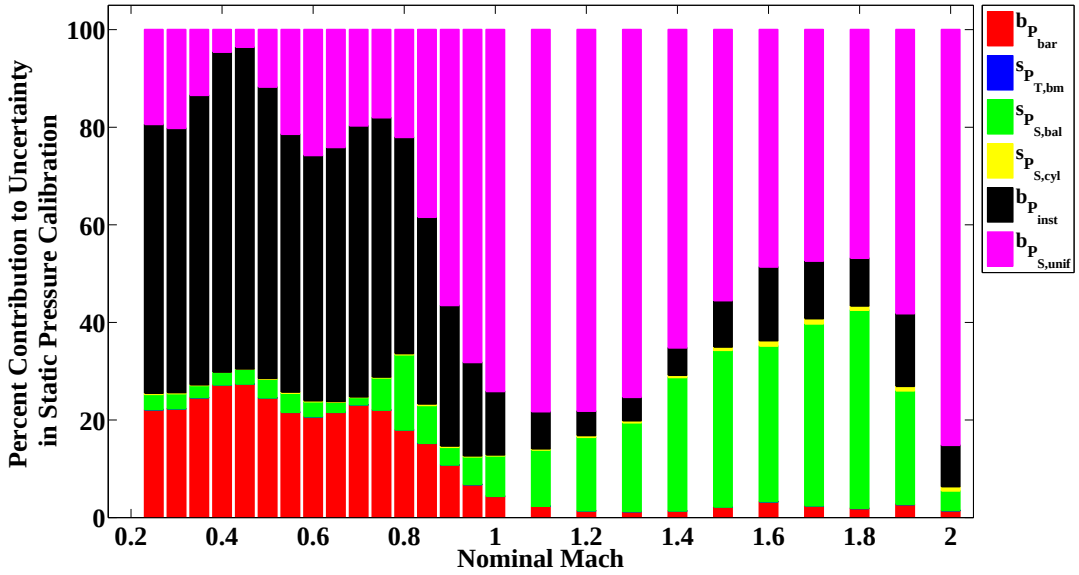

Figure 17: Percent contributions from all sources to the uncertainty of the static pressure calibration as a function of nominal Mach number for test section configuration 1.

Dimensional uncertainty values are presented in the NASA CR.[6] These values are not provided in this publication because as the process changes and the calibrations are performed in the future, the values are expected to change. The CR is updated regularly as the data and analysis evolve and current values are available to the interested public. The percent contributions presented here are sufficient for describing the process and benefits of the analysis, such as possible improvements to the facility uncertainty.

V. Possible Improvements

Arguably the greatest value to performing a ground-up analysis of measurement uncertainty is that the parameters that dominate the overall uncertainty can be determined. It is often of interest to find out how changes in data acquisition, hardware, test matrices, or processes might affect uncertainty. Based on the determined main contributors (or out of sheer curiosity), different "What-If" scenarios are developed to assess their potential impact on uncertainty. These proposed scenarios become hypothetical examples using synthetic data sets, which are created based on the actual data set, and are run through the analysis process that is already established. The synthetic scenario results are then compared to the uncertainty results obtained with actual data.

Scenarios considered in this analysis are:

1. Obtaining more distinct repeat data during the static pressure calibration and examining curve-fit techniques,
2. Replacing total pressure calibration with the assumption $P_{T,bm} = P_{T,ts}$,
3. Replacing current instrumentation with higher accuracy instrumentation, and
4. Using static pressure calibration data from different sources (transonic array vs. cone-cylinder).

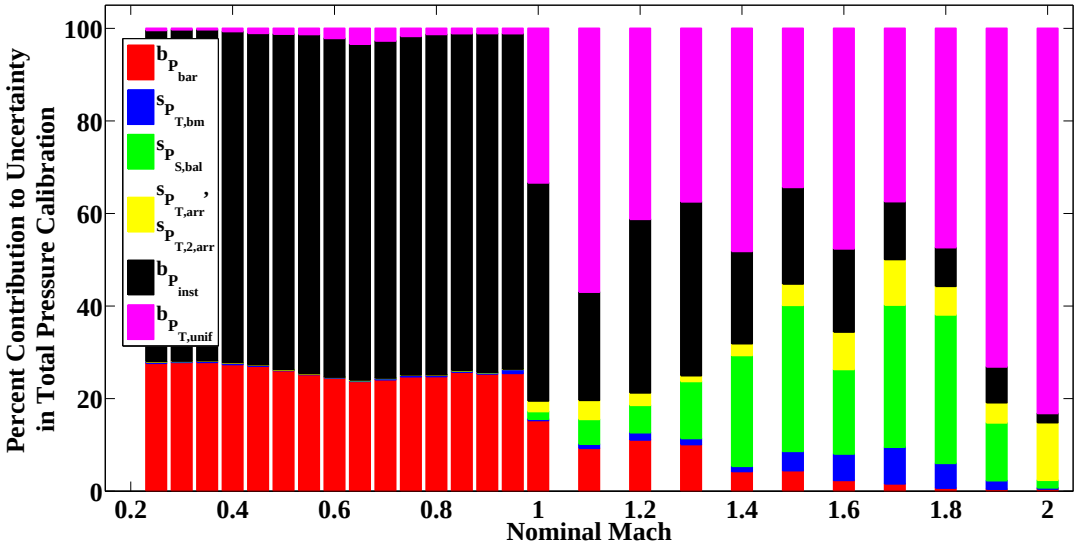

Figure 18: Percent contributions from all sources to the uncertainty of the total pressure calibration as a function of nominal Mach number for test section configuration 1.

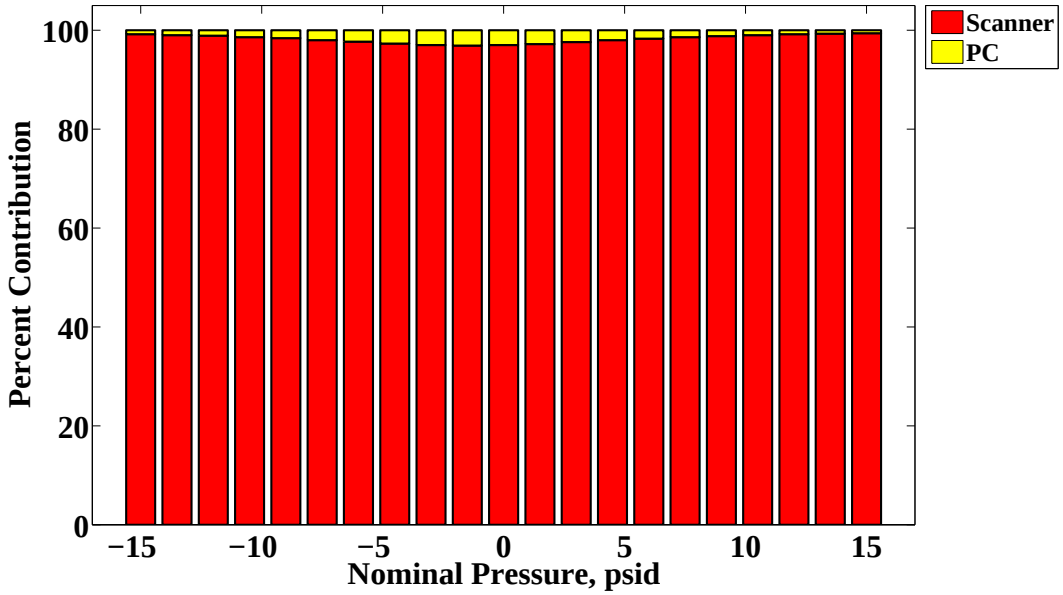

Figure 19: UPC for pressure instrumentation. Red is the pressure scanner and yellow is the PC.

A. Obtaining More Repeat Data During Static Pressure Calibration and Examining Curve-fit Techniques

In theory, uncertainty due to a calibration can be reduced by increasing the distinct (not back-to-back) repeat measurements obtained for each set point used to create a calibration curve. Because this analysis is bottom-up and includes the full calibration uncertainty analysis, simulations of the static and total pressure calibrations are already complete. This scenario of increased static pressure repeat data is considered because results of the analysis indicate that the systematic uncertainty, particularly in the supersonic range are driven by the static pressure calibration (see Figure 16). To simulate this scenario, the input data for the Monte Carlo simulation of static pressure calibration is changed to include n times more repeat measurements.

The simulation is performed for $n = 1$ (original data set), 3, 10, and 30 repeat measurements, taken at each nominal Mach condition (ranging from Mach 0.25-2.0). The simulation performs the curve-fit keeping each data point as a discrete point in the fit. The results are shown in Figure 20. An improvement to combined systematic uncertainty in Mach number is observed as n increases, especially through the supersonic range. Additionally, diminishing returns are observed as n increases; more than three repeat data sweeps have little impact on uncertainty.

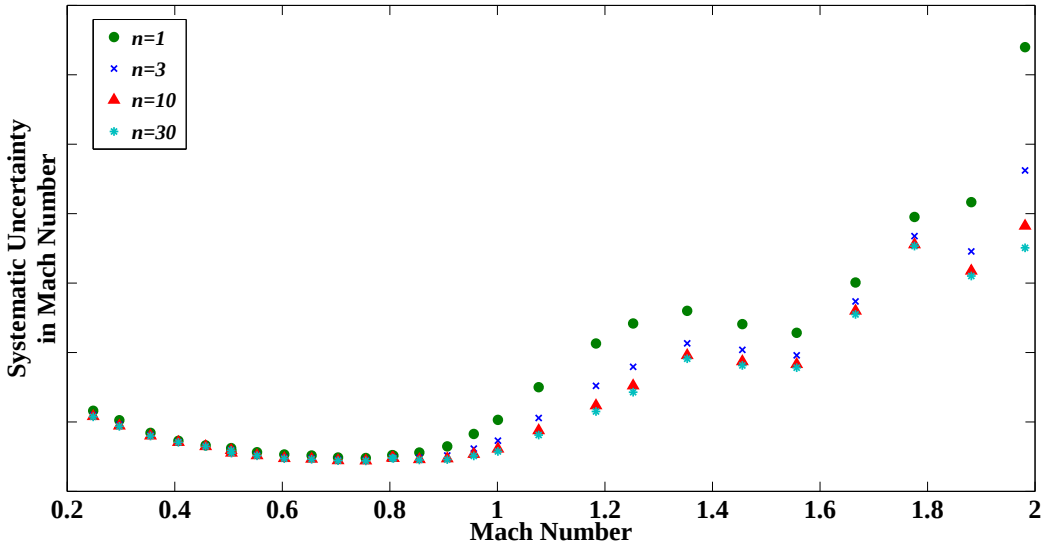

Figure 20: Expanded Systematic Mach Uncertainty: Effect of n times more repeat data points for static pressure calibration, discrete points used for curve-fit in static pressure calibration

It is also of interest to analyze the calibration curve-fit technique to determine if averaging the calculated X and Y components of the fit for repeat measurements before performing the curve-fit impacts uncertainty. Results are shown in Figure 21 using this average-value curve-fit technique. Significant improvement in combined systematic Mach number uncertainty is apparent with $n = 3$ to 10 additional static calibration repeat data points, with diminishing returns as n increases. There appears to be a definite uncertainty advantage to changing the calibration technique by averaging repeat data points before performing the curve-fit; this approach should be further investigated when performing future calibrations and uncertainty analyses.

It should be noted that past calibration data can be added to future calibration tests, creating a collaborative data set, assuming no significant changes have occurred in the facility between calibrations. For example, if 10 overall repeat samples are desired and the present data set includes only 2, the next calibration test matrix could be designed to obtain 8 additional Mach range sweeps of data. Similarly, if calibrations with smaller test matrices could be executed more frequently and designed identically in run sequence, sample size, etc., then the data sets could be smaller but could continue to be combined to increase overall sample size.

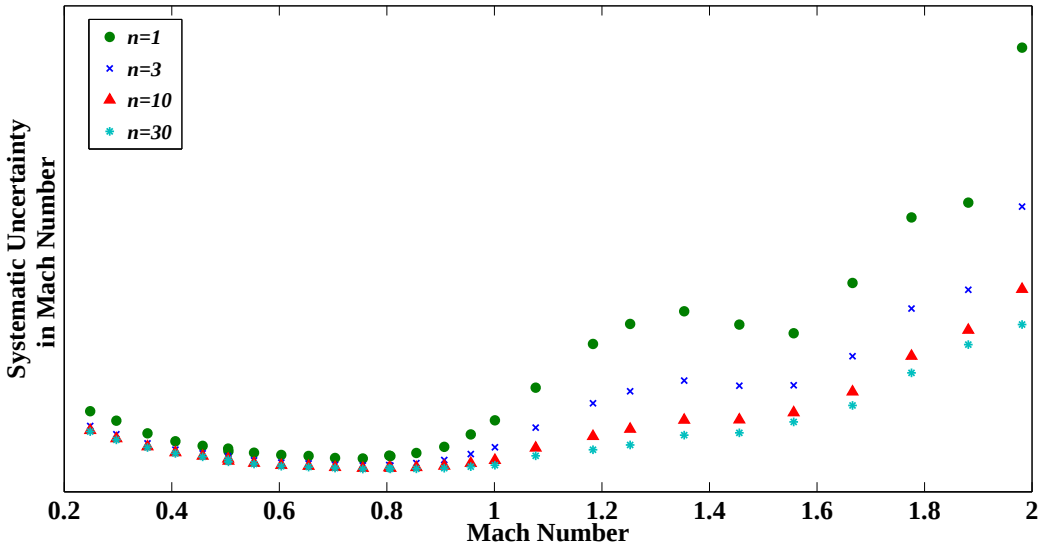

Figure 21: Expanded Systematic Mach Uncertainty: Effect of n times more repeat data points for static pressure calibration, average-value used for curve-fit technique in static pressure calibration

B. Assuming $P_{T,bm} = P_{T,ts}$ in Place of Total Pressure Calibration

When the total pressure calibration test was performed, errors that existed during that calibration test became fossilized into the calibration curve.[10] During a customer test, those fossilized errors propagate as systematic errors into the Mach uncertainty. To reflect this in the simulation, random and systematic standard uncertainties from all measured parameters from the total pressure calibration ($P_{T,bm}$, $P_{T,array}$, and P_{bar}) are estimated and applied, perturbing each parameter by appropriate errors over n Monte Carlo iterations. The result is the "uncertainty contribution from total pressure calibration" to be applied to the calculated $P_{T,ts}$ during a customer test as a systematic uncertainty, containing all fossilized uncertainties from the calibration.

An alternative to total pressure calibration considers the common assumption that the total pressure in the settling chamber (in this facility, the bellmouth) is equal to the total pressure in the test section. It is desirable to determine how Mach uncertainty determined from total pressure calibration curves (and their fossilized uncertainties) compares to the case when calibration is not performed, and other assumptions of test section total pressure behavior are made.

When introducing the scenario that subsonic total pressure calibration is not performed, an estimate should to be made to account for the uncertainty due to the assumption that $P_{T,bm} = P_{T,ts}$. This is explored by first plotting $P_{T,array}/P_{T,bm}$ for all available data points, confirming the average of that ratio across all points is very nearly 1 to validate the assumption. The standard deviation of the actual data sample is evaluated using Equation 8, and results in (for the subsonic example) $s_{P_{T,array}/P_{T,bm}} = 0.0005$. Since the uncertainty needs to be dimensional, the determined standard deviation is multiplied by the test-time $P_{T,bm}$ to provide a valid standard uncertainty to apply to $P_{T,ts}$ in the simulation (see Figure 22). This ends up giving $s_{P_{T,ts}} = 0.0005 * P_{T,bm}$ as the uncertainty in $P_{T,ts}$ due to the assumption. This uncertainty estimate replaces the entire fossilized total pressure calibration uncertainty (see Figure 23). Using the same general approach supersonically, the uncertainty to apply to $P_{T,ts}$ is $s_{P_{T,ts}} = 0.0035 * P_{T,bm}$.

Results of the scenario assuming $P_{T,ts} = P_{T,bm}$ can be seen in Figure 24. In the subsonic flow range, both approaches show a similar uncertainty result. Supersonically, it proves advantageous to use calibration curves in the range of Mach 1.1-1.6, but it is noted that the assumption provides a better uncertainty for Mach 1.8-2.0. Results of this scenario indicate that for this facility, the calibration curves ought to remain in use unless a customer wishes to test at the top of the facility's range, at which point they should be aware that it may be beneficial to replace the calibrated total pressure with the assumption of $P_{T,ts} = P_{T,bm}$.

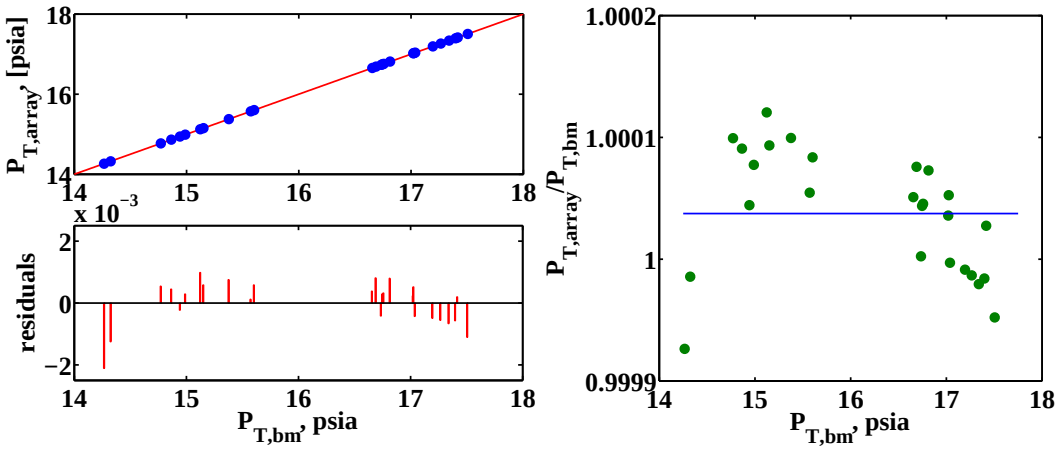

Figure 22: (left) Subsonic total pressure linear curve-fit and residuals; (right) Scatter represents $P_{T,array}/P_{T,bm}$ of raw data, line represents the average of all points ($\cong 1.0000$)

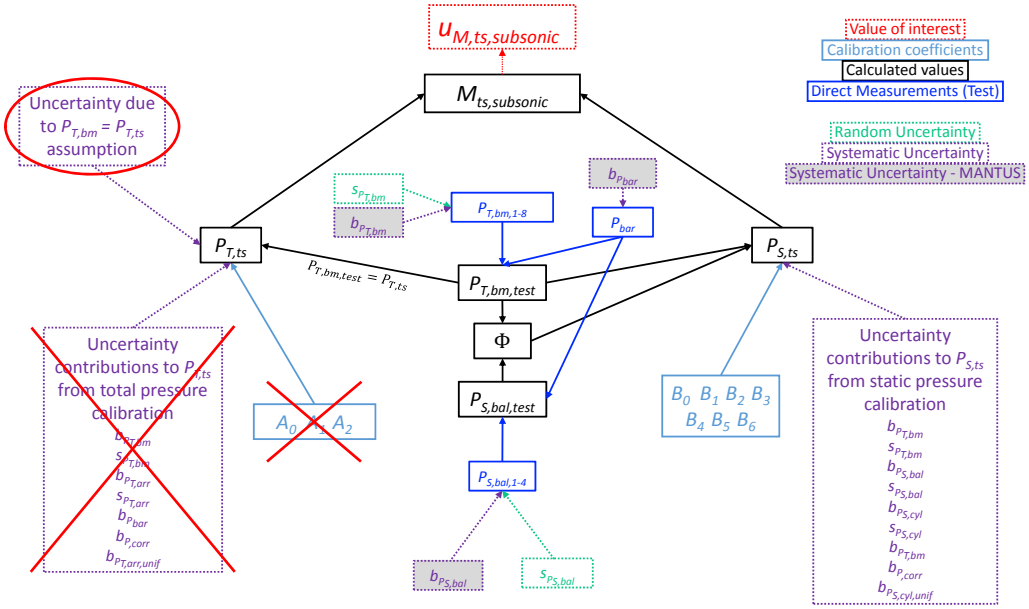

Figure 23: Uncertainty Flow Chart for Subsonic Total Pressure Calibration: Modified for $P_{T,bm} = P_{T,ts}$ Assumption

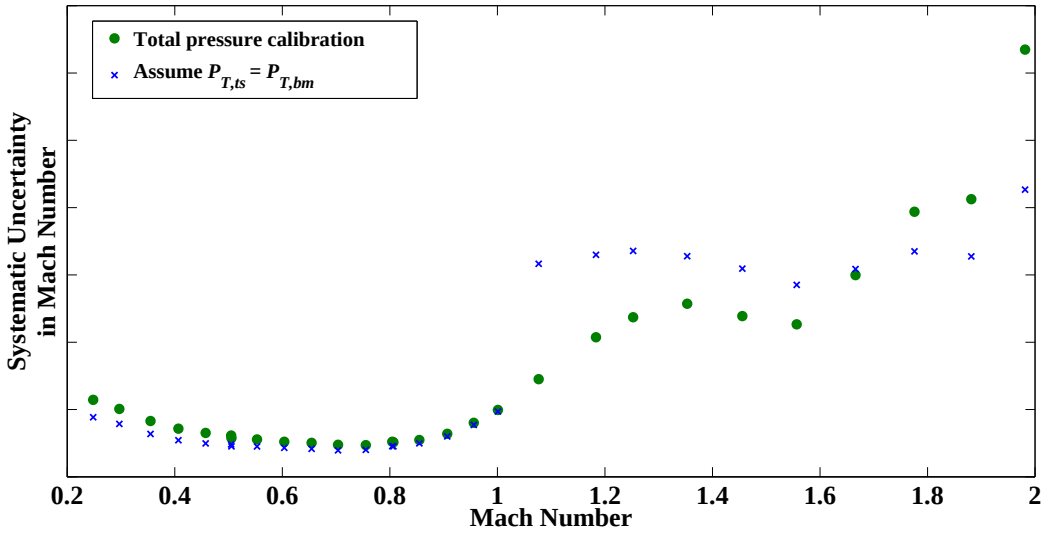

Figure 24: Mach Uncertainty: Effect of Total Pressure Calibration compared to $P_{T,ts} = P_{T,bm}$ Assumption

C. Replacing Current Instrumentation with Higher Accuracy Instrumentation

A high accuracy instrument is often equated with a low measurement uncertainty. But this often is not the case in complex measurement systems, as the following example shows. A simulation is performed to investigate what the Mach uncertainty impact is if all pressure transducers have a stated accuracy of 0.02% reading, as opposed to 0.03-0.04% full scale, which is typical of the ESP system. This scenario also assumes re-calibration of the tunnel after hardware changes. Results of this scenario can be seen in Figure 25. There is a slight improvement to systematic uncertainty in Mach number through the subsonic range of the tunnel. Since the current drivers to systematic uncertainty in Mach number in the supersonic range are due to spatial uniformity during calibration, there is little benefit to making such a costly instrumentation change. Unless other major systematic uncertainty contributors were addressed first, this change would have little effect over most of the facility's test range.

D. Using Static Pressure Calibration Data From Different Sources (Transonic Array vs. Cone-Cylinder)

The calibration data obtained during the 1996-1997 calibration test included test section static pressure measured by both the cone-cylinder (currently used for static pressure calibration curve) and from the transonic array. In the calibration's data analysis, the presence of apparent shock interaction effects on the array static pressures made use of the data undesirable. Even though shock effects were also present in the cone-cylinder data, it was concluded that the cylinder data would be a better representation of tunnel static pressure behavior than the array, and that the shock effects would average out when data from the aft half of the cylinder was used.

A modified simulation is performed to analyze use of array static pressures. A calibration curve based on array static pressures is created and applied to the calculation of $P_{S,ts}$. The data is analyzed to obtain the array static pressure standard uncertainty estimate in the same manner other uncertainty parameters are determined. A comparison is made with the current static pressure calibration (using cone-cylinder data and its uncertainties) to see which provides a more desirable uncertainty outcome. Results of this comparison can be seen in Figure 26. Results indicate the current use of cone-cylinder data is far superior to the array data. This is found to be a result of the influence of static pressure uniformity uncertainty; the impact of the spatial non-uniformity is much lower for the cone-cylinder since the effect is averaged out over 56 ports, and has a higher impact on the transonic array where only 7 measurements were averaged. This scenario is a good reminder that calibration and uncertainty teams must work closely to ensure the data choices made during calibration are beneficial for maintaining calibration integrity, while also being mindful of their

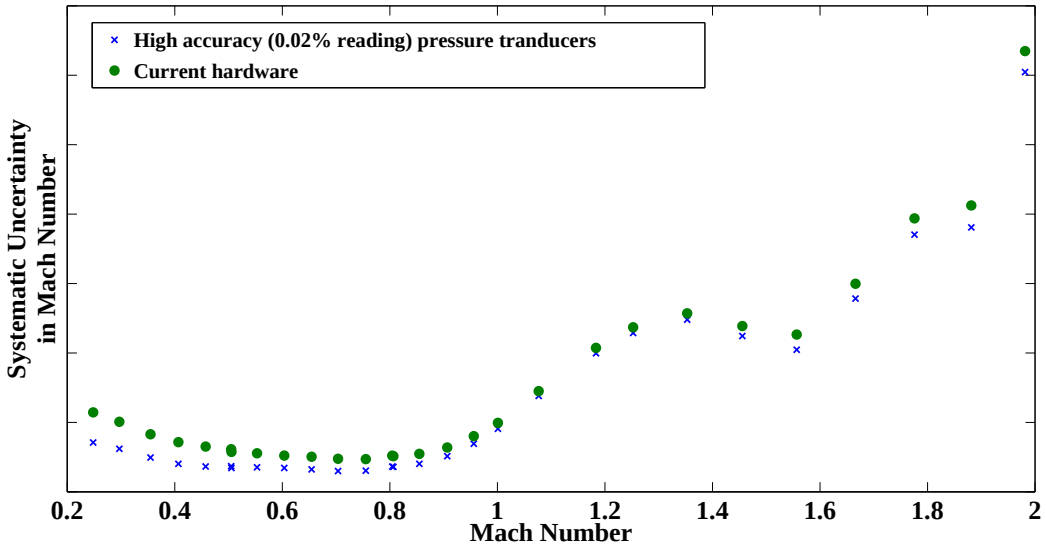

Figure 25: Mach Uncertainty: Effect of Replacing Current Instrumentation with High Accuracy Instrumentation

impact on uncertainty.

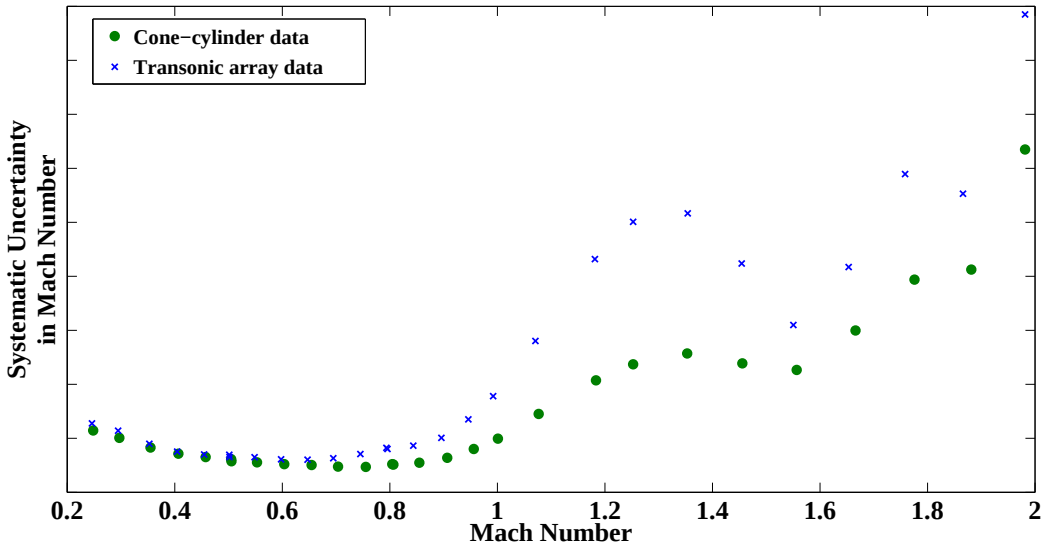

Figure 26: Mach Uncertainty: Effect of using different data sources for static pressure calibration

E. Summary of Scenarios

A summary of all of the scenarios performed and their results is shown in Table 2. This table can be used by the facility personnel to improve facility uncertainty through facility upgrades or changes to calibration and test time practices in the future.

Scenario	Result
Obtain more distinct repeat data during static pressure calibration and change curve-fit technique	Up to 60% decrease in Mach number systematic uncertainty through supersonic regime
Assume $P_{T,bm} = P_{T,ts}$ instead of using total pressure calibration curve	Total pressure calibration curve is superior, except from Mach 1.8-2.0 where a 15-30% decrease in Mach number systematic uncertainty was noted with use of the assumption
Replace pressure instrumentation with higher accuracy instrumentation (0.02% reading)	Little benefit since other sources currently drive systematic uncertainty in Mach number
Use static pressure measured by the transonic array vs. cone-cylinder for calibration	Current calibration data from cone-cylinder is far superior; systematic uncertainty in Mach number is up to 100% higher using the array

Table 2: Mach number "What-If Scenarios" summary

VI. Conclusion

An uncertainty analysis was performed on the 8- by 6-foot Supersonic Wind Tunnel at NASA Glenn Research Center. The complexity of the data reduction process made a faithful replication of it impractical using traditional Taylor Series error propagation techniques. As a result, the Monte Carlo Method of propagating uncertainty was selected.

Uncertainties were classified as random (variability about the mean value) and systematic (offset of average measured value from the true value) to aid users in determining which uncertainties are of interest for specific tests. Uncertainty sources were determined and elemental uncertainty estimates were made for all considered sources. Instrumentation uncertainties were estimated using MANTUS,[11] an Excel® based tool tailored for modularized instrument systems to determine the combined uncertainty of an instrument. Random uncertainties and spatial uniformity uncertainty were estimated using data from the most recent tunnel calibration.[5] All uncertainties considered in the analysis were propagated from the point of measurement through the instrumentation, data system, tunnel calibrations and finally data reduction to arrive at the uncertainty in the calculated test section Mach number. Results were analyzed and broken down at every step so that a comprehensive understanding of driving uncertainty sources could be determined.

Correlation effects and a small repeatability data set were two challenges faced in this analysis. Measurements were correlated due to the instrumentation and/or operation of the facility. For example, the facility set point was based on the ratio of $P_{S,bal}$ to $P_{T,bm}$. As a result, there was a seemingly wide variation in each of these parameters, while the ratio stayed fairly constant at any given set point. This translated to an unrealistically large random uncertainty estimate when the correlation was not properly accounted for. The statistical analyses, engineering judgments made to account for correlations, and other challenges faced were discussed in this document.

The percent contribution of uncertainties were presented. The break down of random vs. systematic uncertainties and the various contributions to each were shown. This break down enables researchers to determine the effect uncertainties will have on the validity of their tests, and aids facility personnel in improving the facility. The primary driver to Mach number uncertainty is the systematic uncertainty due to the static pressure calibration.

Scenarios were developed and simulated to deduce their potential improvements to Mach number uncertainty. Table 2 summarizes the notable results of the scenarios explored. These scenarios and conclusions enable facility personnel to make educated improvements such as those presented in Table 3 as they consider facility upgrades and plan future calibration tests.

Sources that drive uncertainty	Actions suggested to mitigate their impact
$s_{P_{S,bal}}, s_{P_{T,bm}}$	Random uncertainty needs to be understood more fully in this facility. A facility study using a test matrix with at least 5-10 repeat Mach sweeps and identical hardware setup for both the transonic array and cone-cylinder should be considered to begin to achieve this understanding. Customers desiring better repeatability than quoted should plan repeat data points in their own test matrices.
b_{PSCAL}, b_{PTCAL}	Calibration test matrices should include at least 3 full Mach range sweeps for critical calibration points (i.e., tunnel center-line).

Table 3: Summary of uncertainty mitigation factors

References

[1]American Society of Mechanical Engineers. "Test Uncertainty". Standard ASME PTC 19.1-2013, 2014.

[2]American Institute of Aeronautics and Astronautics. "Assessment of Experimental Uncertainty with Application to Wind Tunnel Testing". Standard AIAA S-071A-1999, 1999.

[3]Joint Committee for Guides in Metrology. "Evaluation of Measurement Data - Guide to the Expression of Uncertainty in Measurement". Guide JCGM 100:2008, International Organization for Standardization, 2008.

[4]S. Castrup and H.T. Castrup. "Measurement Uncertainty Analysis Principles and Methods: NASA Measurement Quality Assurance Handbook - ANNEX 3". Handbook NASA HDBK 8739.19-3, National Aeronautics and Space Administration, 2010.

[5]E. A. Arrington. "Calibration of the NASA Glenn 8- by 6-foot Supersonic Wind Tunnel". Calibration Report NASA/CR-2012-217270, National Aeronautics and Space Administration, January 2012.

[6]J. Stephens, E. Hubbard, J. Walter, and T. McElroy. "Uncertainty Analysis of the NASA Glenn 8x6 Supersonic Wind Tunnel". Contractor report, National Aeronautics and Space Administration, In Progress.

[7]R. H. Soeder. "NASA Glenn 8-by 6-foot Supersonic Wind Tunnel User Manual". Technical Memorandum NASA TM 105771, National Aeronautics and Space Administration, 1993.

[8]Ames Research Staff. "Equations, Tables, and Charts for Compressible Flow". Technical Report NACA TR-1135, National Aeronautics and Space Administration, 1953.

[9]H. W. Coleman and W. G. Steele. *Experimentation, Validation and Uncertainty Analysis for Engineers*. John Wiley and Sons, Inc., Third edition, 2009.

[10]R.J. Moffat. "Describing the Uncertainties in Experimental Results". *Experimental Thermal and Fluid Science*, Vol. 1(No. 1), 1988.

[11]B. Rouse, J. Morales, and T. McElroy. "Measurement Analysis Tool for Uncertainty in Systems Overview". Contractor report, National Aeronautics and Space Administration, In Progress.

[12]J.L. Devore. *Probability and Statistics for Engineering and the Sciences*. Brooks/Cole, Fifth edition, 2000.

[13]Joint Committee for Guides in Metrology. "Evaluation of Measurement Data - Supplement 1 to the "guide to the Expression of Uncertainty in Measurement" - Propagation of Distributions using a Monte Carlo Method". Supplement JCGM 101:2008, International Organization for Standardization, 2008.

[14]J. Walter, W. Lawrence, D. Elder, and M. Treece. "Development of an Uncertainty Model for the National Transonic Facility". Technical Report AIAA 2010-4925, American Institute of Aeronautics and Astronautics, 2010.